Nonlinear Analysis for Investigating Seismic Performance of a Spun Pile-Column of Viaduct Structure

A. Fajar Setiawan [1*] , A. Kurniawan Santoso [1], M. Fauzi Darmawan [1],
Agus Darmawan Adi [1], Sito Ismanti [1]

[1] Department of Civil and Environmental Engineering, Faculty of Engineering, Universitas Gadjah Mada, Yogyakarta 55281, Indonesia.

Abstract

Slab-on-pile SOP viaducts have been constructed on several highways and railways in Indonesia, but there are certain doubts about some practical structural seismic design concepts. Therefore, this study aims to investigate the seismic performance of a single spun pile column for the SOP viaduct using nonlinear analysis. The essential variables used include the effect of top pile reinforced concrete infill treatment, soil-pile structure interaction (SPSI), and different response modification factors (R). Moreover, the single spun pile column was designed as a macro model with a force-based beam-column element having a fiber section in the plastic hinge. The static pushover analysis and quasi-static cyclic were also conducted to determine the displacement limit state and the equal viscous damping, respectively. Furthermore, seven pairs of ground motion excitations were used to investigate seismic performance in line with ASCE 7-10 and ASCE 61-14. The results showed that the implementation of the top-pile reinforced concrete infill treatment slightly reduced seismic response but evoked more severe pile curvature in the embedded zone. In addition, the behavior and seismic performance were slightly better than those without treatment when considering the SPSI. This study recommends the spun pile column for the SOP viaduct with a response modification factor of 1.5 to avoid probable brittle failure occurrence under earthquake load.

Keywords: Soil-Pile Structure Interaction; Response Modification Factor; Displacement Limit State; Hysteretic Energy.

1. Introduction

Several highway and railway infrastructures were constructed recently, particularly in Indonesia, to accelerate economic growth. The slab-on-pile (SOP) viaduct was observed to be popular as a continuous elevated track in both infrastructures due to its simple structural configuration and fast construction method [1]. The typical configuration of the SOP structure consists of the spun pile functioning as the viaduct pier, and then the foundation, pile head, and concrete slab, as presented in Figure 1. It is similar to the wharf structure, where the lateral seismic resistance is usually supported by the extended pile foundation as a column. Some of the advantages of using these spun piles, also known as prestressed hollow section concrete piles, include material durability, an easy construction process, and an economical cost.

Indonesia currently has no specific standard structural design for SOP structures with spun pile columns. This is the reason its seismic design is based on the SNI 2833:2016 [2] standard adopted from AASHTO LRFD (2012) and normally applied to bridge structures [3]. Moreover, there is no provision regarding spun pile column utilization, while the ASCE 61-14 [4] standard was formulated for the seismic lateral resistance of using prestressed piles for the wharf structure.

Most Indonesian practical engineers currently use linear analysis methods such as static equivalent and response spectrum, which involve introducing response modification factors (R) to determine the nonlinear performance of bridge structures, including SOP [5]. However, this nonlinear performance tends to vary depending on the capacity of the structures to reserve strength (overstrength) and dissipate energy (ductility). The trend was also noted by Mahmoudi & Zaree (2010) [6], who noted that the structural ductility and energy dissipation capability significantly influenced the response modification factor of a structure. The study further showed that both SNI 2833:2016 [2] and AASHTO LRFD (2012) [3] offered the response modification factor of 1.5, 3.5, and 5 for critical, essential, and other categories, respectively, in multiple column bents of the other bridge design. Several structural design reports observed showed that some SOP viaducts were designed using R-values of 3 and 5, even though ASCE 61-14 [4] required a seismic response modification factor of 2 for prestressed piles. It was noted that this factor of 2 was used to design a wharf structure at Nabire Port, Indonesia [7]. This means the adoption of ASCE 61-14 [4] was more appropriate than the AASHTO LRFD (2012) [3] for the structural design of SOP.
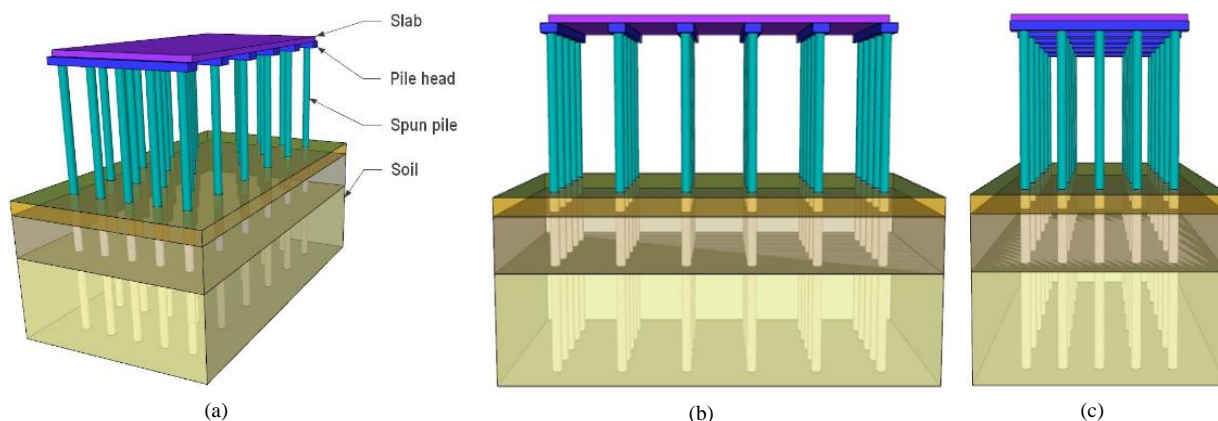

Figure 1. An overview of SOP structural configuration in the study: (a) 3D view, (b) longitudinal view, and (c) transversal view

Several studies have been conducted on the seismic resistance and structural behavior of spun piles. For example, an experimental study showed that the spun pile without any treatment produced low energy dissipation and ductility [8], and this was further confirmed by a pinching hysteresis loop applied by Setiawan et al. (2020) [9]. Benzoni et al. (1997) [8] also observed that the pinching behavior of the tested specimen was affected by the high initial stiffness provided by the prestressing bar. Furthermore, the application of a more significant axial load to the top pile produced a lower equal damping capacity, which was below 10%. It is important to note that these significant deficiencies of spun piles have not been considered in the structural design of SOP. This was observed from the findings of Cofer et al. (2009) [10] that implementing top pile treatment with reinforced concrete infill was the best solution to overcome the weakness of using spun pile in the SOP viaduct for the high seismic region. The finite element simulation applied in the study showed that the tensile crack propagated through roughly 90% of the reinforced concrete infill area up to the moment of failure in the concrete infill instead of the hollow spun pile [10]. However, there is presently no full-scale experimental test and evident nonlinear analysis of the spun pile for the SOP viaduct. It was also discovered that the former study did not consider the interaction between soil and pile, and this can affect the appearance of the plastic hinge formation, thereby indicating the pile-column failure. This means there is a need to conduct an appropriate nonlinear structural analysis to capture those problems.

This study applied the nonlinear analysis to a single spun pile column of a slab-on-pile (SOP) viaduct structure to investigate the behavior and seismic performance of different structural treatments, important categories, and idealizations. The focus was on several essential variables, such as the effect of top pile treatment with reinforced concrete (RC) infill and different applications of the response modification factor (R). Moreover, the difference in the effect of using bottom-fix restraint on bottom-pile restraint effects was also studied with due consideration for the soil-pile structure interaction (SPSI). The first process involved validating the numerical model through the simulation of the experiment conducted on a full-scale soil pile under a quasi-static lateral loading test by Hutchinson et al. (2004) [11]. The preliminary simulation was intended to evaluate the accuracy and validity of the numerical model of the laterally loaded embedded pile using OpenSees software with due consideration for the soil-pile structure interaction. Furthermore, the main study formulated some monotonic and cyclic laterally loading analysis scenarios for the extended single-spun pile-column model of the SOP viaduct structure. It is also pertinent to state that the SPSI model idealized the soil springs as the p-y model. Moreover, nonlinear time history analysis was applied to obtain the structural dynamic responses under the designed earthquake excitations. The seismic performance of top spun pile treated with reinforced concrete infill was also studied, while the effect of SPSI and different response modification factors (R) implemented was also investigated in relation to the plastic hinge formation, hysteretic loop characteristics, and structural seismic performance.

2. Methods

A numerical model validation was first conducted followed by the investigation of the structural behavior and seismic performance of extended single pile-column models using the research method briefly explained in the following Figure 2.
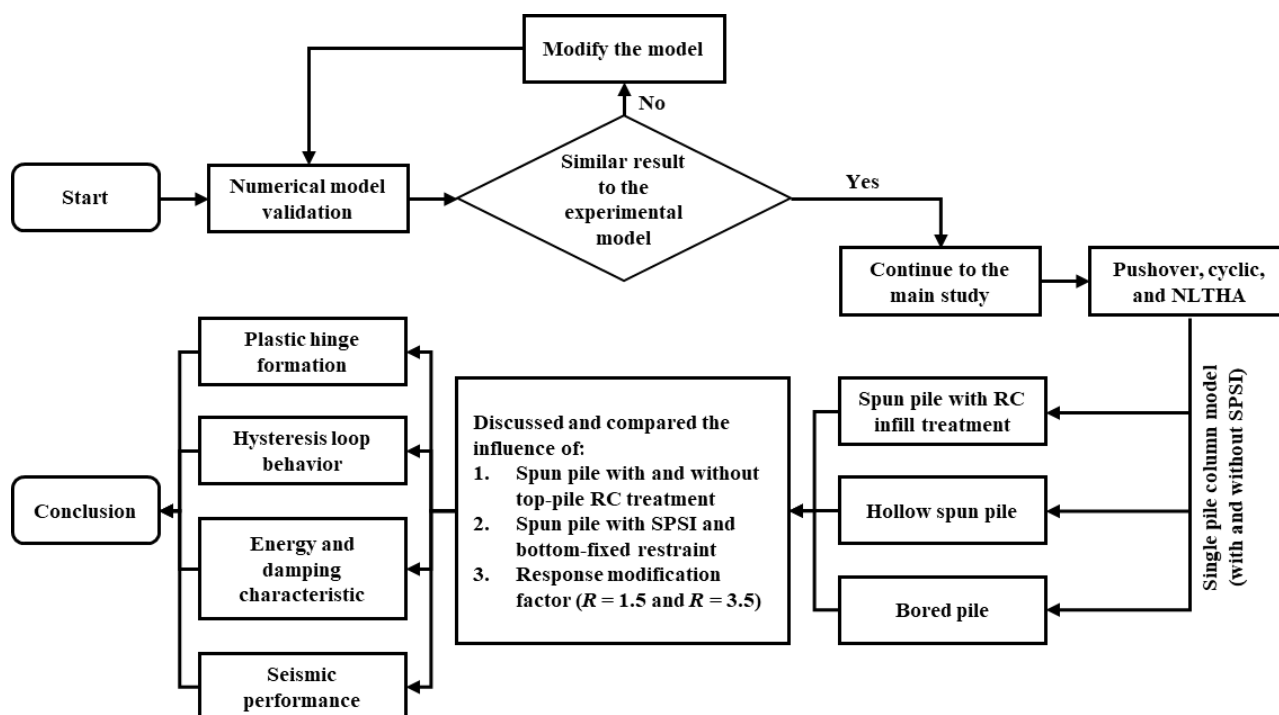

Figure 2. The research flowchart

A numerical model validation was first conducted on an extended pile-shaft structure with reference to the experimental studies by Hutchinson et al. (2004) [11] and Chai & Hutchinson (2002) [12]. These studies only considered a top-free single pile model, which led to the addition of a top-fixed restraint pile model to represent the connection between the pile and pile cap. The validation process showed a good agreement in the hysteresis loop with the former experimental result, which means it was possible to apply the same modeling method to the main study.

The main study was conducted by designing three types of single pile-column models, including hollow spun pile, spun pile infilled with reinforced concrete, and RC bored pile, using different response modification factors of $R = 1.5$ and $R = 3.5$. Moreover, the RC bored pile models were developed to compare the behavior and seismic performance of the spun pile. It is also important to note that the effect of soil-pile structure interaction (SPSI) was compared to the bottom-fixed restraint at the end of the fixity depth. Several analyses were conducted, including pushover, cyclic, and nonlinear time history analysis (NLTHA). The static-monotonic pushover analysis was used to determine the capacity curve of the single pile column; the quasi-static cyclic analysis was applied to generate the hysteresis loop; and the nonlinear time history analysis (NLTHA) was used to investigate the structural responses under the designed earthquake excitations. The results obtained were in the form of the plastic hinge formation, hysteresis loop behavior, energy dissipation, equal viscous damping, and seismic performance of each model, which were discussed and compared. The intention was to provide an appropriate suggestion and the best choice for practicing engineers in the process of designing SOP viaduct structures with spun pile columns.

2.1. Numerical Model Validation

The single pile model used for the validation was developed according to Hutchinson et al. (2002) [11] and Chai and Hutchinson (2002) [12] that conducted a full-scale soil-pile lateral loading test to investigate the extended pile-shaft structure with a focus on the lateral strength, cyclic behavior, and ductility capacity. The test pile embedded in a large soil container is presented in the following Figure 3-a, and axial pressure was applied using two high-strength steel tie-down rods, each loaded with a hydraulic jack. Moreover, an actuator reacting against a large-capacity reaction block provided the lateral force for the cyclic loading test. Pile Test No. 4 was simulated using OpenSees [13] through the application of the Scientific Toolkit for OpenSees (STKO) [14] as the pre-processor and post-processor. The specimen had an above-ground height of $6D$ and was embedded in loose dry sand to a depth of $13.5D$ from ground level, where D is the diameter of the pile. The axial force, P, of 445 kN was also applied to represent the nominal axial stress level of $0.1f'_c$, where f'_c is the uniaxial compressive strength of the concrete.
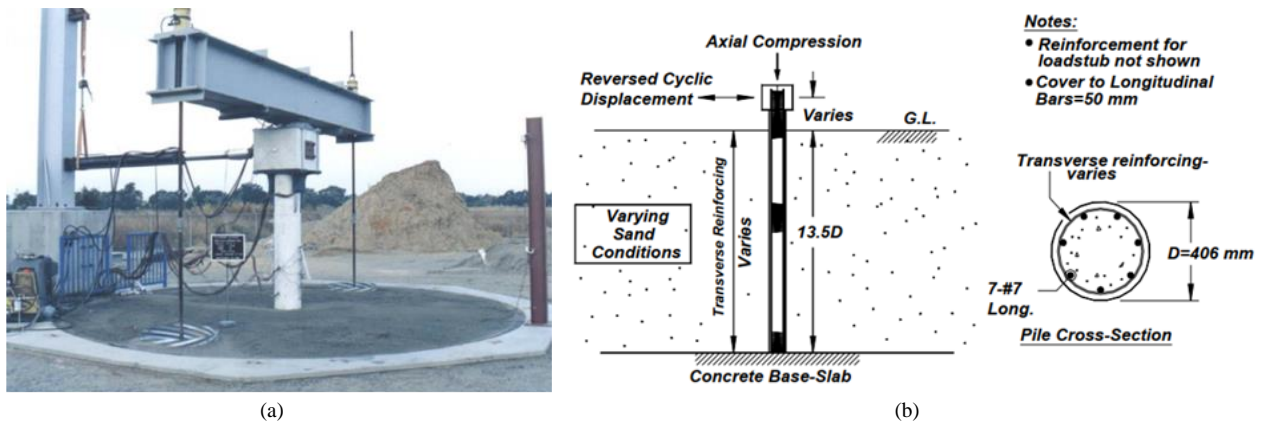
Figure 3. An experiment test by Hutchinson et al (2002) [13]: (a) the setup and (b) the reinforcement details of the tested pile

The study also used seven Grade A706 ϕ22 bars (d_b = 22.2 mm) as the longitudinal reinforcement with a well-defined yield stress of f_y = 421 MPa as indicated in the details of the pile specimen presented in Figure 3-b. It was also discovered that the MW45 smooth wire (d_{sp} = 7.3 mm) at 50 mm pitch provided concrete confinement while the transverse steel had an equivalent yield stress estimated at 605 MPa. Moreover, the concrete material provided a compressive strength, f'_c, of 47.5 MPa while the soil used for the test had average wet density and friction angle of 17 kN/m^3 and 37°, respectively.

A two-dimensional numerical model was developed for the test pile using STKO-Opensees software as shown in Figure 4-a. The pile had displacement-based beam-column elements and fiber sections, and a P-delta with a large displacement effect was considered by applying the corotational geometric transformation. Furthermore, the stress-strain relationship of the concrete material was based on the Modified Kent and Park model [15] through the utilization of the Concrete02 material in the OpenSees material library as presented in Figure 4-b. The constitutive model of the longitudinal steel material was designed using Steel01 and MinMax materials in the OpenSees material library as indicated in Figure 4-c.
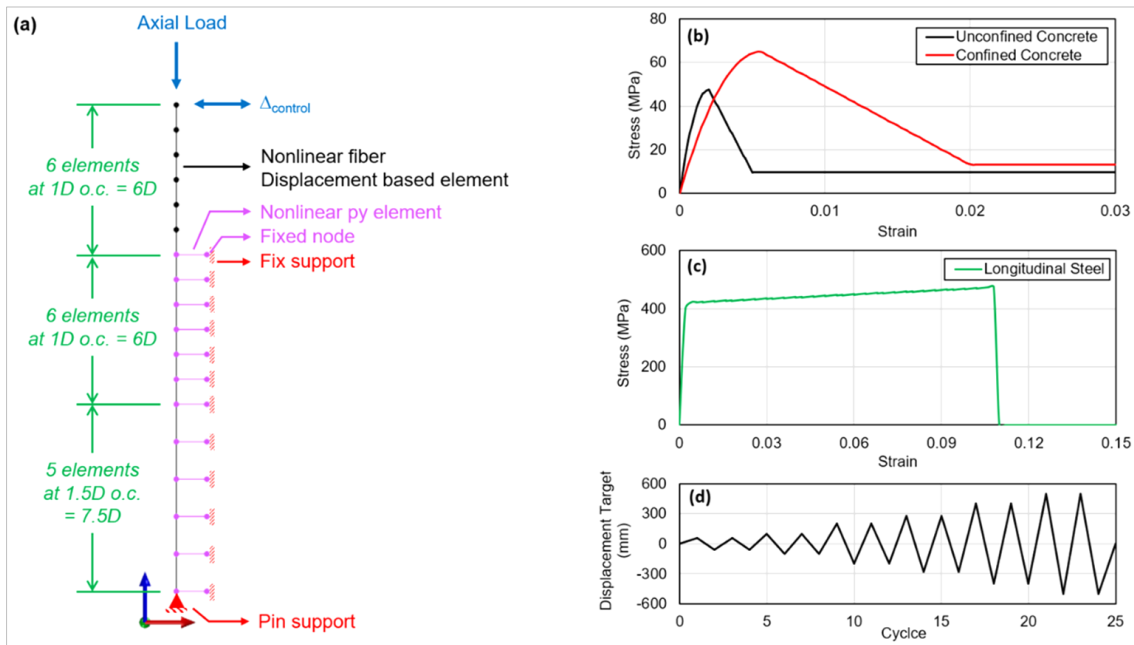

Figure 4. Illustration of (a) structural idealization of the numerical model and a constitutive model of (b) concrete, (c) longitudinal steel bars, and (d) cyclic loading protocol

The soil-pile structure interaction in the numerical analysis was considered using a nonlinear p-y spring element. It is also important to note that the p-y curve for cohesionless soil without liquefaction presented in API (2007) [16] was adopted. Moreover, the PySimple1 material provided in OpenSees, as explained by Boulanger et al. (2003) [17], was utilized to construct the soil spring material. The pin restraint was assigned to the bottom node of the pile, while the fixed restraint was assigned to the fixed node of the spring element. The process involved two conditions and the first was that the top node was assumed to be rotation-free to represent the experimental condition, while the second was that the rotation at the top node was fixed to represent the SOP piles condition connected to a rigid pile head and slab.

The axial and cyclic lateral push loads were employed at the top node based on the cyclic loading protocol presented in Figure 4-d. It is pertinent to state that the cyclic loading analysis was applied after the gravity analysis and was used to produce the hysteretic loop. The numerical result obtained after the whole process was later compared to the experimental test data to assess its accuracy.

2.2. Main Study of Numerical Modeling for the Extended Single Spun Pile-Column in SOP

The main study was used to conduct a nonlinear analysis of single pile-column models of SOP using the STKO-OpenSees software. The spun pile with reinforced concrete (RC) infill treatment and bored pile models were initially redesigned to provide an equivalent seismic resistance to the existing structure which was in the form of a hollow spun pile model. It is important to note that the redesigned models were developed in a previous study by Darmawan et al. (2022) [18] based on SNI 2833:2016 [2] which is equivalent to AASHTO LRFD (2012) [3]. Moreover, the single pile-column configuration was calculated using static equivalent and response spectrum methods in line with the provision of the code. The maximum demand/capacity (D/C) ratio of all models was observed to be in the range of 0.7 to 0.9 as previously noted by Darmawan et al. (2022) [18]. The configuration for each of the pile-column models is presented in Figures 5-b to 5-d.
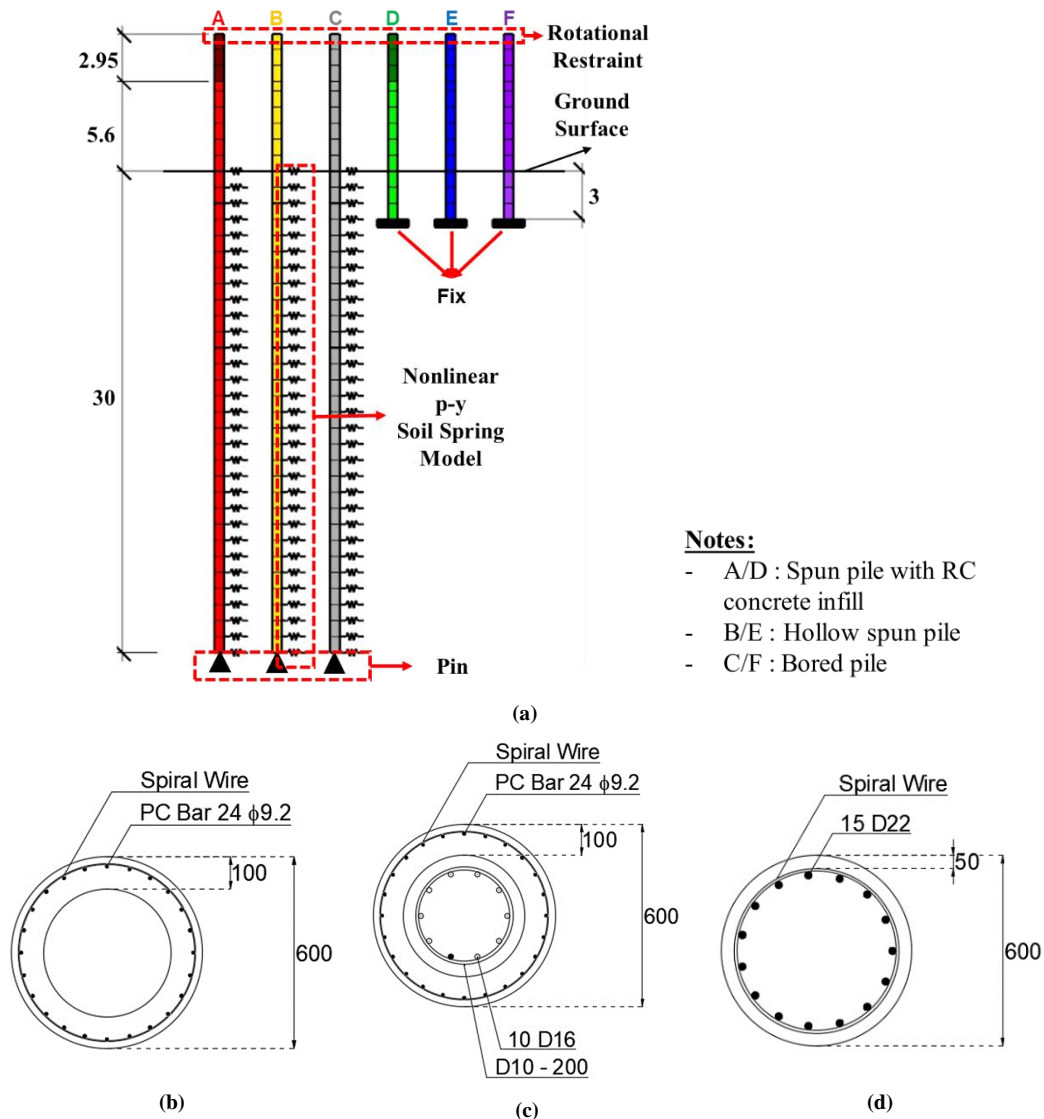

Figure 5. Modeling schemes for the single pile-column: (a) single pile models idealization (unit in m), (b) hollow spun pile (unit in mm), (c) spun pile infilled with reinforced concrete (unit in mm), and (d) bored pile (unit in mm)

The three groups of the proposed models are shown in Figure 5. The first group was Models A and D, the spun piles equipped with top-pile concrete infill treatment with due consideration for the soil-pile structure interaction (SPSI) and bottom-fixed restraint, respectively. The second was a hollow spun pile designed based on SPSI (Model B) and bottom-fixed restraint (Model E), and the third was a single reinforced concrete (RC) bored pile model accompanied by SPSI (Model C) and bottom-fixed support (Model F). The piles with SPSI were designed to have a total length of 38.55 m,

out of which 8.55 m was the free-standing pile length. Furthermore, the embedded pile lengths were 30 m and 3 m for the models designed with due consideration for the SPSI and the bending moment inflection point depth, respectively. It is also important to state that the reinforcing steel area ratio in the concrete infill treatment was 1.6%.

The influence of response modification factor variation was also considered in the designed pile. This was indicated by the application of 1.5 and 3.5 as the factors for the critical and essential bridge based on the operational categories according to SNI 2833:2016 [2], which is also equivalent to AASHTO LRFD (2012) [3]. Moreover, the preliminary design of the SOP structure led to a variation in the additional mass of the superstructure applied to the top pier depending on the response modification factor used. The additional axial load assigned for all types of pile sections to represent the superstructure loads distributed on the top is indicated in Table 1 in addition to the moment and shear capacity.

Table 1. Axial load and moment & shear capacity of the pile sections

Pile Section	P (kN)		P / ($A_g f'_c$)		Moment Capacity (kNm)		Shear Capacity (kN)	
	R 1.5	R 3.5	R 1.5	R 3.5	R 1.5	R 3.5	R 1.5	R 3.5
Hollow spun Pile			1.65%	3.06%	394.85	375.79	171.72	171.73
Spun Pile + RC Infill	141.3	261.3	1.18%	2.19%	495.90	482.54	266.88	266.90
Bored Pile			1.67%	3.08%	389.33	370.16	238.13	238.13

The spun pile was composed of concrete material with a compression strength f'_c = 54.4 MPa, while the concrete infill had a maximum compression stress of 27.03 MPa, and the bored pile had an unconfined concrete strength of 30 MPa. These values were idealized using Concrete02 as proposed by the Modified Kent-Park model (Scott et al., 1982). Moreover, Steel01 was used to idealize reinforcements and prestressed bar materials with certain limits, using MinMax material to represent the failure. The steel bar had a yield stress of 420 MPa, while the prestressed concrete had 1387 MPa. It is pertinent to note that the initial prestressing effect was also considered using the initial strain material.

The single piles were modeled as displacement-based beam-column elements (DBE), while the sections were discretized as fibers to represent the material nonlinearity at the sectional area. The plastic hinge was assumed to spread along the element using the Gauss-Lobatto integration rule because the yielding could potentially occur at a specific location along the pile length due to the different lateral stiffness provided by each SPSI's link. Meanwhile, deeper fixity produced higher stiffness, and this led to the construction process using zero-length elements every 1 m starting from ±0.00 m to -30.00 m elevation, with the parameters of the p-y material for the pile embedded in the sand determined based on API (2007) [16]. The bottom pile of the model designed with SPSI consideration was restrained in translation (pin) based on the assumption that there was no settlement.

Several idealizations of parameter input were considered for the nonlinear time history analysis. For example, the mass and load were localized at each node along the pile length in the lump idealization in order to simplify the mass matrix used in the dynamic analysis. Meanwhile, a rotational restraint was applied to the top pile to represent the pile head restraint. The geometric nonlinearity with P-delta plus large displacement was also considered for the axial force applied to the top pile, and this had the ability to increase the internal forces in the same way as the stress in the pile element [19].

2.3. Structural Behavior and Performance Evaluation

Nonlinear static procedures were applied to simulate the nonlinear behavior of the pile models using pushover and cyclic analysis. The pushover analysis was used to determine the capacity curve and the plastic hinge formation after reaching a specific target displacement. Moreover, several limit states were applied to the curve to determine the pile's capacity under several performance levels in line with ASCE 61-14 [4]. The performances were categorized into three levels, including minimal damage, controlled damage, and life safety protection, and these were applied based on the concrete strain limit according to the provision code. The limit states and the description are summarized in Table 2. It is important to note that the limit state for the prestressed pile was addressed in the ASCE 61-14 provision. The actual limit state was possibly more stringent for the spun pile (hollow section prestressed pile) with low confinement, thereby, leading to a potential explosive brittle failure [20].

Table 2. Limit states for pile according to ASCE 61-14 [4]

Performance Level	Description	Concrete Strain Limit
Minimal damage	The structure performs near elastic behavior with minor or without residual deformation.	$\varepsilon_c \leqslant 0.004$
Controlled damage	The structural behavior is still controlled or repairable, although limited inelastic behavior occurs.	$\varepsilon_c \leqslant 0.006$
Life safety protection	The unpreventable damage occurs, but the structure can withstand support gravity loads.	$\varepsilon_c \leqslant 0.008$

The cyclic analysis was used to capture the pile's hysteresis behavior. This was represented by the equivalent viscous damping and hysteretic energy which were used to compare the structure's dissipating capability between the six models. The hysteretic energy (A_h) was an area of the complete cycle in the hysteretic response while the equal viscous damping (ξ) was calculated by equating the hysteretic energy with the absorbed energy as shown in Equation 1 [21] where F_m and Δ_m are the maximum force and displacement in each cycle, respectively.

$$\xi = \frac{A_h}{2\pi F_m \Delta_m} \tag{1}$$

The other parameters, initial stiffness, and maximum lateral strength, were also compared to determine the difference in the hysteresis loop characteristics of each model. The initial stiffness was calculated by dividing the initial force by the initial displacement as presented in the tangent method. The calculation was made using the parameters obtained from the hysteresis loop and they were also used as indicators to show the influence of several variables considered in this study. Moreover, the maximum lateral strength was obtained from the peak lateral resistance monitored in the backbone curve. The dynamic responses of the structure were obtained through nonlinear time history analysis after which seven pairs of ground motions recorded were selected in line with the provision of ASCE 7-10 [22].

The selection process was based on several criteria including the fault type, magnitude (M_w), fault distance (R_x), and condition of the Yogyakarta earthquake site. It is significant to note that the site was categorized as class E based on the SOP structure's standard penetration test result (Kulon Progo, Indonesia). The fault type was found to be strike-slip based on the Opak fault in Yogyakarta, Indonesia. The de-aggregation result for the Yogyakarta zones also showed that the magnitude of the earthquake was 6.8 with a fault distance of 17 km. Furthermore, a single scale factor was calculated based on each response spectral within the period of interest and the values obtained were multiplied by each ground acceleration to generate the scaled ground motions as presented in Table 3.

Table 3. Records of the selected seven ground motion

No	Earthquake	Station	M_w	R_x (km)	V_{s30} (m/s)	Scale Factor (S.F.)
1	Chichi	CHY047	6.20	38.6	169.5	3.5
2	Darfield	Christchurch	7.00	18.1	187	2.5
3	El Mayor	Botanical Gardens Meloland, E Holton Rd.	7.20	30.2	196	2.0
4	Imperial Valley	El Centro Array #3	6.53	10.8	162.9	2.0
5	Morgan Hill	Hollister City Hall	6.19	30.8	198.8	5.5
6	Tottori	SMN002	6.61	16.6	138.8	2.9
7	Victoria	Chihuahua	6.33	18.5	242.1	2.5

The seismic performance of the single extended spun pile of the SOP structure was investigated by comparing the maximum top-pile displacements obtained from the dynamic analysis to the limit states at the capacity curve determined using static analysis. The monitoring process required the control of the top pile displacement with the strain and deformation of section hinges in both top and bottom locations. The mean of the seven dynamic responses was considered according to the ASCE 7-10 [22].

3. Results and Discussion

3.1. Validation Analysis Results

The validation analysis showed that the initial stiffness and strength degradation of the numerical simulation coincided with the experimental result as indicated in Figure 6-a. Meanwhile, the lateral strength from the numerical simulation was about 18% lower than the value obtained from the experimental test. This means the findings were sufficiently coincident. It was also discovered that the two scenarios for each monotonic pushover and cyclic loading analysis were performed by considering the top node of the pile as free and fixed restraint of moment rotation. The top fixed restraint moment idealization was used to investigate the effect of the pile group action on the actual implementation of the SOP viaduct system. The cyclic loading analysis result for both scenarios is presented in Figure 6-b. The findings showed that the top fixed restraint idealization of the pile provided significantly higher structural strength up to 1.8 times compared to the top-free condition.
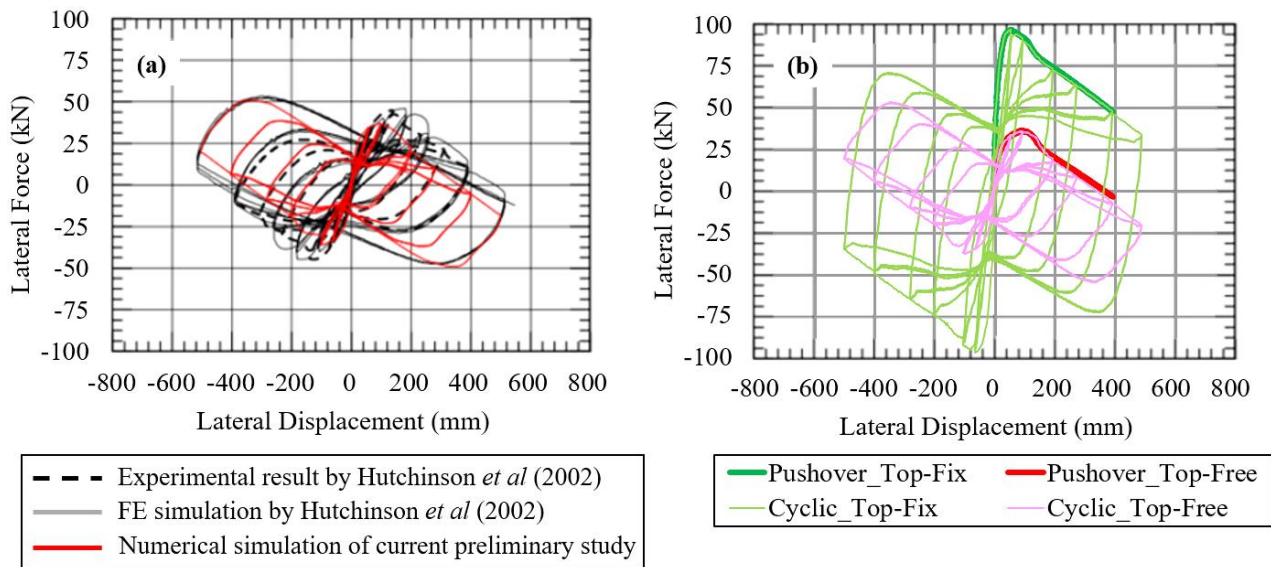
Figure 6. (a) Validation results according to Hutchinson et al. (2002) [12] and (b) extended cyclic analysis

3.2. Main Study Results

3.2.1. Plastic Hinge Formation of a Spun Pile Column

The numerical analysis showed that more plastic hinge curvature was generated in the embedded zone of the spun pile with RC infill treatment on the top compared to the specimen without the treatment, as indicated in Models A and B in Figure 7. The top plastic hinge of Model A was found to have a larger bending strength capacity, and this forced more severe plastic hinge formation in the bottom zone. It is important to note that the bottom plastic hinge was the original hollow spun pile section and had lower bending strength than the top hinge with concrete infill. Moreover, the inclusion of reinforced concrete infill as a treatment during the process of implementing the bottom fixed restraint was able to reduce the plastic rotation of the top hinge, as shown in the comparison of Model D and E in Figure 7. This means practical engineers should be aware of the effect of the concrete infill treatment on the top pile region in the process of designing structures due to its ability to provoke more severe plastic hinge formation in the embedded zone.

The plastic hinge curvature of SPSI models in the life safety limit state was visible at the top pile and slightly at the embedded zone, as shown in Figure 7. Meanwhile, the bottom-fixed restraint models, D, E, and F, dominantly showed the plastic curvature near the bottom moment fixed restraint and emerged slightly at the top pile. The phenomenon was influenced by the stiffness produced by the different support idealizations.
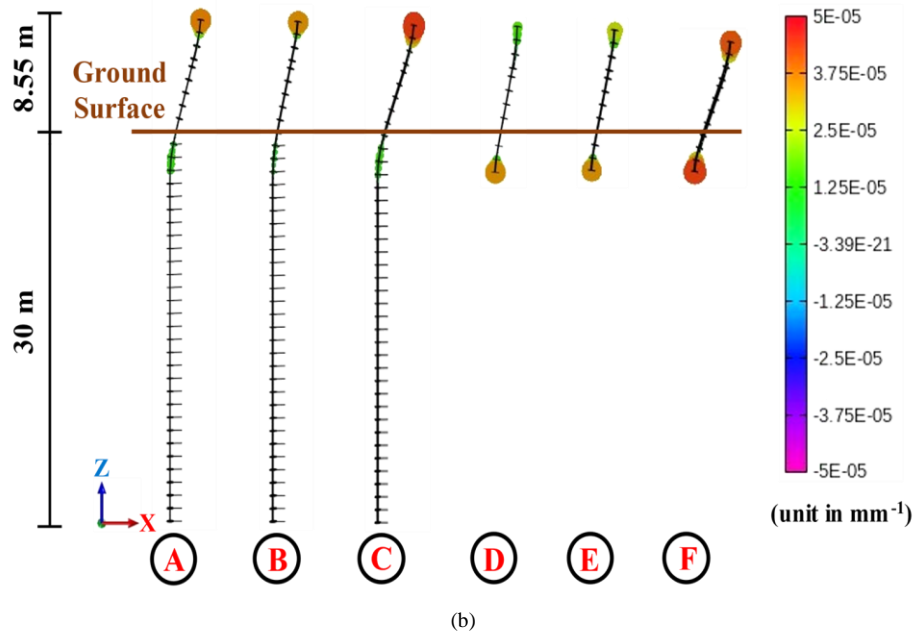

(a)

(b)
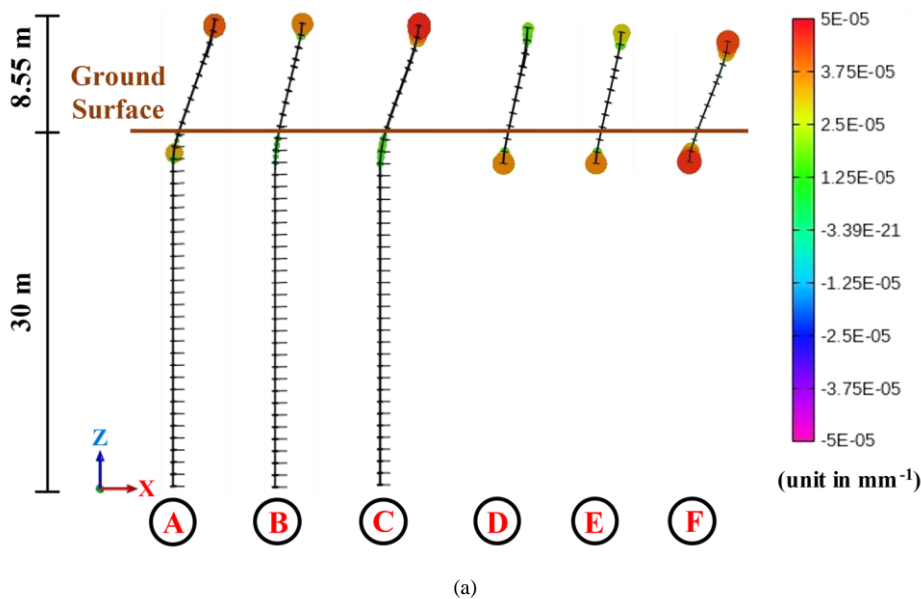
Figure 7. Plastic hinge curvature formation of the designed pile with different response modification factors (*R*); (a) response modification factor (*R*) of 1.5 and (b) response modification factor (*R*) of 3.5

It is important to note that the bottom-fixed restraint was the translation and rotation through extremely high stiffness or fully rigid assumption, preventing the base from lateral displacement and causing a significant concentrated plastic curvature around the fixed rotation restraint location. Meanwhile, the SPSI consideration in Models A, B, and C generated lower lateral resistance and restrained moment distribution, thereby, allowing more widespread light plastic hinge formation in the embedded zone. The process also triggered the dominant concentrated plastic hinge formation in the top zone, which was restrained by the fixed rotation. However, the response modification factors did not exhibit a significant difference in plastic hinge formation on the piles. Model A with a top pile and RC infill treatment generated less curvature in the bottom hinge when 3.5 was used as an *R*-value instead of 1.5.

3.2.2. Hysteretic Loops Behavior

The numerical simulation showed that different variations of the designed pile produced different lateral strengths under cyclic loading, as shown in Figures 8 and 9 as well as Table 4. It was discovered that the lateral strength capacity of the spun pile with reinforced concrete infill treatment on the top was slightly increased by 11.75% than the specimen without the treatment [23]. However, the hysteretic loop's shape and immensity remained identical. Orientilize et al. (2021) [24] compared three specimens of the spun pile with a diameter of 450 mm through pushover and cyclic analysis, and the findings showed the ability of the additional reinforced concrete infill with 6D19 rebar to increase the lateral strength by up to 45%. The other parameter, which was the difference in compression strengths of infilled concrete at 35 MPa and 50 MPa, did not show significant differences in the spun pile lateral strength. Meanwhile, the findings of this present study indicated a slight increase in the lateral strength of the spun pile with reinforced concrete infill because the probable plastic hinge occurred at the top and bottom zones. It was also discovered that the bottom plastic hinge used the hollow spun pile section. Models A and E were enhanced with reinforced concrete infill treatment, but the bottom plastic hinge was found to be the weakest, and this governed the lateral strength of the pile.

(a)   (b)
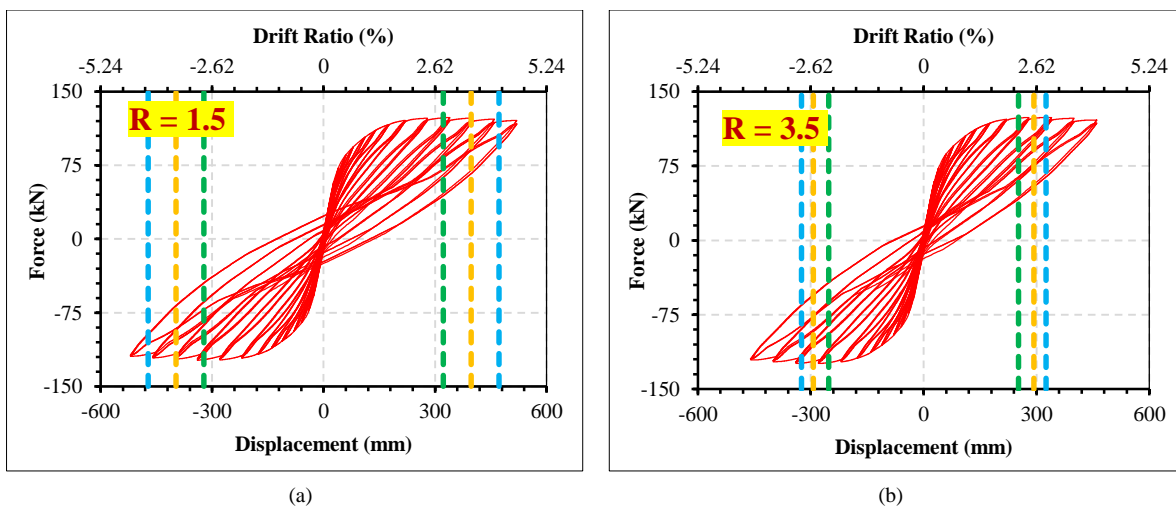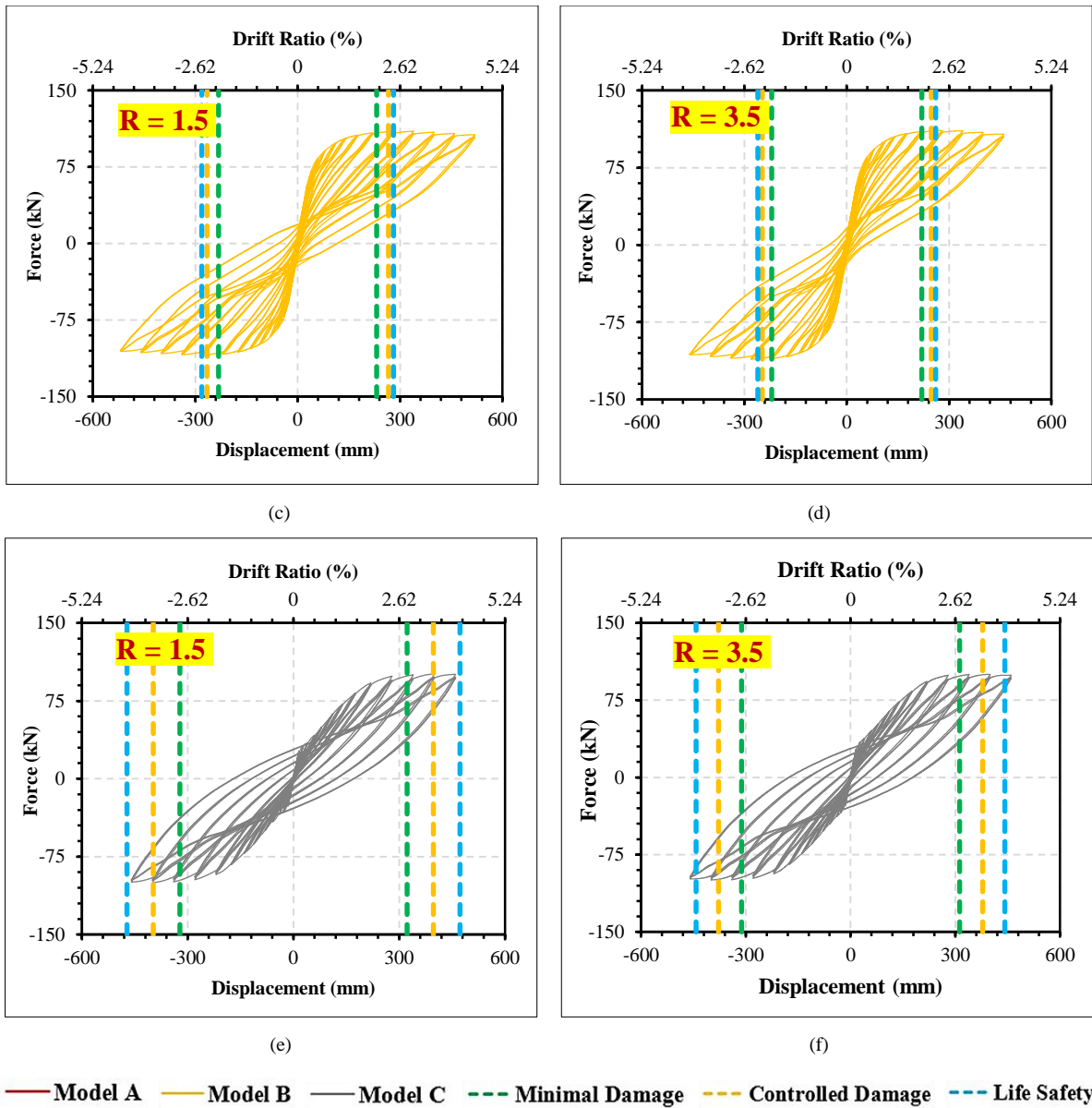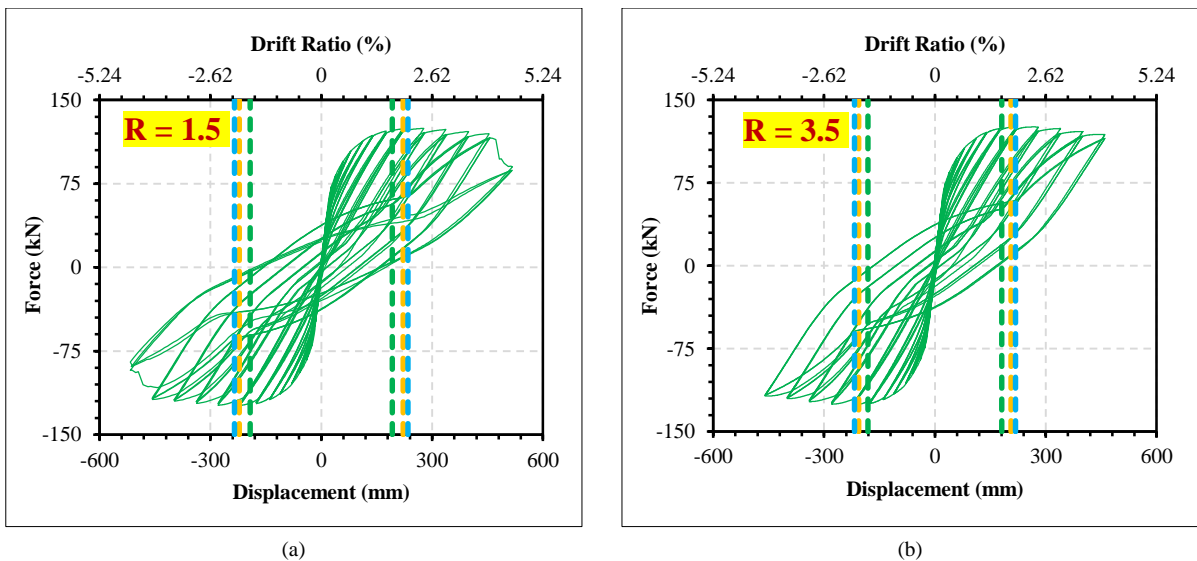
Figure 8. The force-displacement curve of SPSI models under cyclic loading: (a) Model A – R = 1.5, (b) Model A – R = 3.5, (c) Model B – R = 1.5, (d) Model B – R = 3.5, (e) Model C – R = 1.5, (f) Model C – R = 3.5
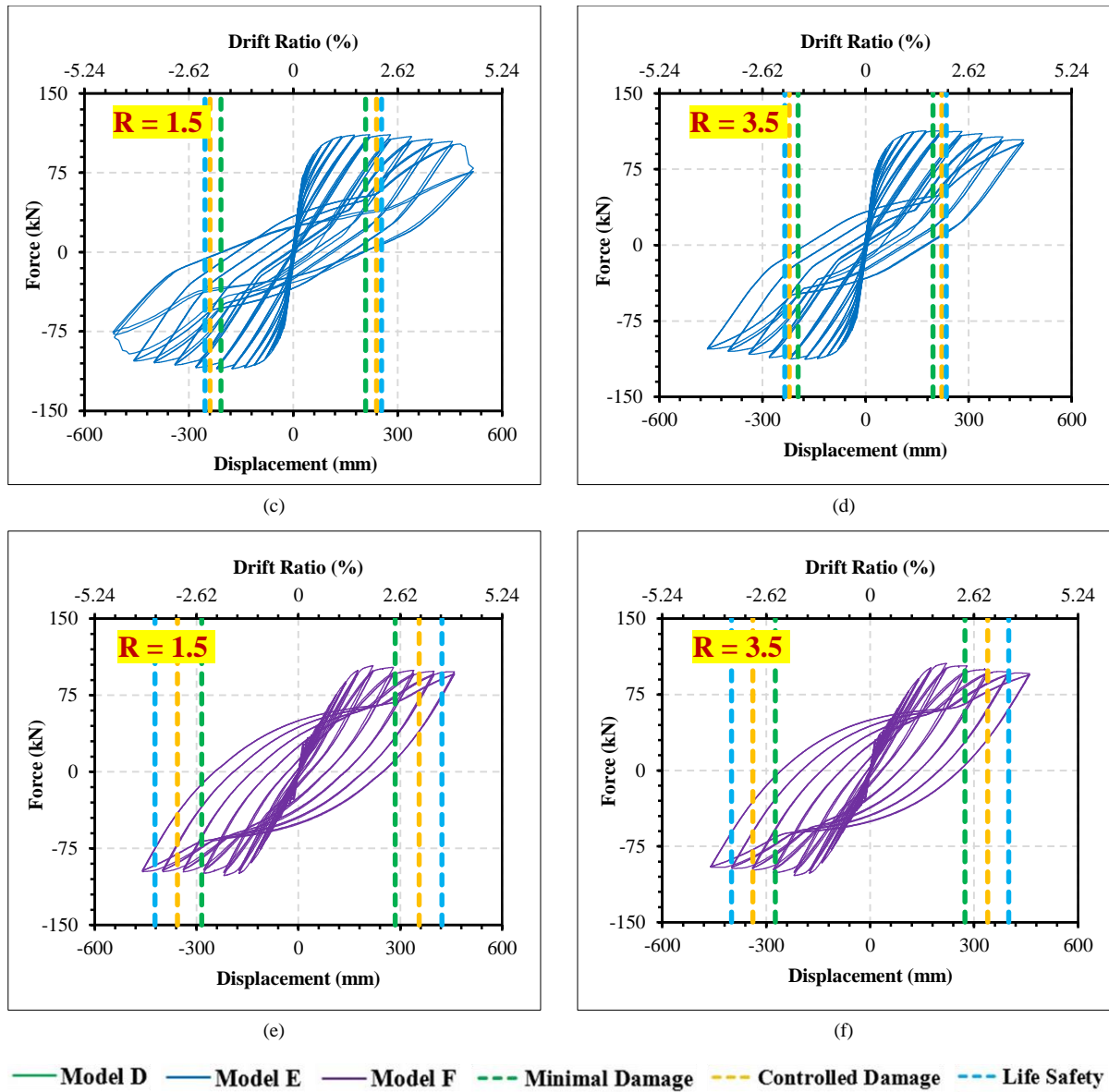
Figure 9. The force-displacement curve of bottom-fixed restraint models under cyclic loading; (a) Model D – R = 1.5, (b) Model D – R = 3.5, (c) Model E – R = 1.5, (d) Model E – R = 3.5, (e) Model F – R = 1.5, (f) Model F – R = 3.5

Table 4. Hysteresis loop parameters of each model

Model	R	Initial stiffness (kN/m)	Maximum lateral strength (kN)	Minimal damage limit displacement (mm)	Controlled damage limit displacement (mm)	Life safety limit displacement (mm)
A	1.5	2109.87	120.67	322	397	472
	3.5	2103.13	120.01	252	293	325
B	1.5	2067.49	108.35	232	266	281
	3.5	2064.81	107.38	220	248	261
C	1.5	1130.08	102.08	322	397	471
	3.5	1685.27	100.72	312	378	442
D	1.5	2606.01	121.69	192	222	235
	3.5	2671.22	120.56	181	206	218
E	1.5	2571.11	111.15	208	239	254
	3.5	2637.69	109.18	196	222	235
F	1.5	1208.98	105.36	285	356	423
	3.5	2115.57	104.69	274	339	400

The bored pile models, C and E, produced the lowest elastic stiffness with more significant energy dissipation and equal viscous damping. This was indicated in Table 4 which was used to represent the parameters of the hysteresis loop in Figures 8 and 9. It was further discovered that the bored pile models were able to perform large hysteresis loops without any pinching behavior. This was in line with the findings of El-Arab & Maki (2012) [25] that there was almost no pinching on the hysteresis loop when conducting experiments using the circular reinforced concrete column pile under cyclic loading. Meanwhile, severe pinching was observed in the hollow spun pile as well as the other pile with reinforced concrete infill treatment. This also aligned with Yang et al. (2018) [26], who elucidated the pinching behavior of spun piles with different reinforcement configurations, including prestressing and additional deformed bars. Their findings further noted that more severe pinching occurred on the spun pile with only prestressing bars. It was also reported that the pinching behavior of the additional deformed bars was not severe, and the energy dissipation capacity increased with the quantity and area.

The analysis of the SPSI showed that its lateral stiffness was lower than the idealization of a bottom-fixed restraint as presented in Table 4, but the strength capacity was almost the same. It was also discovered that SPSI displayed better post-yield stability than the bottom-fixed restraint when subjected to large displacements of greater than 2%, but its hysteresis loop was narrower. This was due to its more widespread hinge formation, which generated lighter plastic rotation and produced a narrower hysteretic loop, unlike the bottom-fixed restraint model with a more concentrated hinge formation.

The observation of the limit states applied with the sectional strain monitored showed that the SPSI models had more significant lateral displacement limits than the bottom-fixed restraint models, as indicated in Table 4. This was due to the fact that the SPSI produced a more flexible structure than the bottom-fixed restraint, which led to a longer deformation in the equal limit state. Moreover, the bottom zone pile plastic hinge of the SPSI models was longer and more widespread than the bottom-fixed models. The consideration of the SPSI in the spun pile model with RC infill treatment on the top (Model A) allowed the generation of a longer displacement limit than the specimen without treatment (Model B). Meanwhile, the spun pile model with bottom-fixed restraint and pile top treatment with RC infill reduced the displacement limit.

The application of different response modification factors significantly affected the displacement limit state as shown in Figures 8 and 9 as well as Table 4. However, it was discovered that the hysteresis loop for the models with 1.5 and 3.5 was almost equal due to the occurrence of axial stress in the light level at a value less than $0.2A_gf'_c$, as shown in Table 1. The findings also showed that the models with a factor of 1.5 achieved a more significant displacement limit state than those with 3.5. This means a smaller response modification factor has the capacity to produce a higher deformation capacity against severe earthquakes as well as the ability to produce a pile with a stable post-yield behavior due to the smaller axial load under the nonlinear geometry effect. Nevertheless, the application of a smaller response modification factor required more piles to obtain an equivalent seismic capacity for the force demanded.

3.2.3. Energy Dissipation and Equal Viscous Damping Characteristics

The results showed that the implementation of top pile treatment with RC infill did not provide a significant difference from the hollow spun pile regarding the equal viscous damping and hysteretic energy as indicated in Figure 10. This was found to be in line with the results of Callista et al. (2022) [27] that the pinching hysteretic loops of a hollow spun pile and another model with reinforced concrete infill treatment were identical, thereby, indicating similar energy dissipation between the two models.
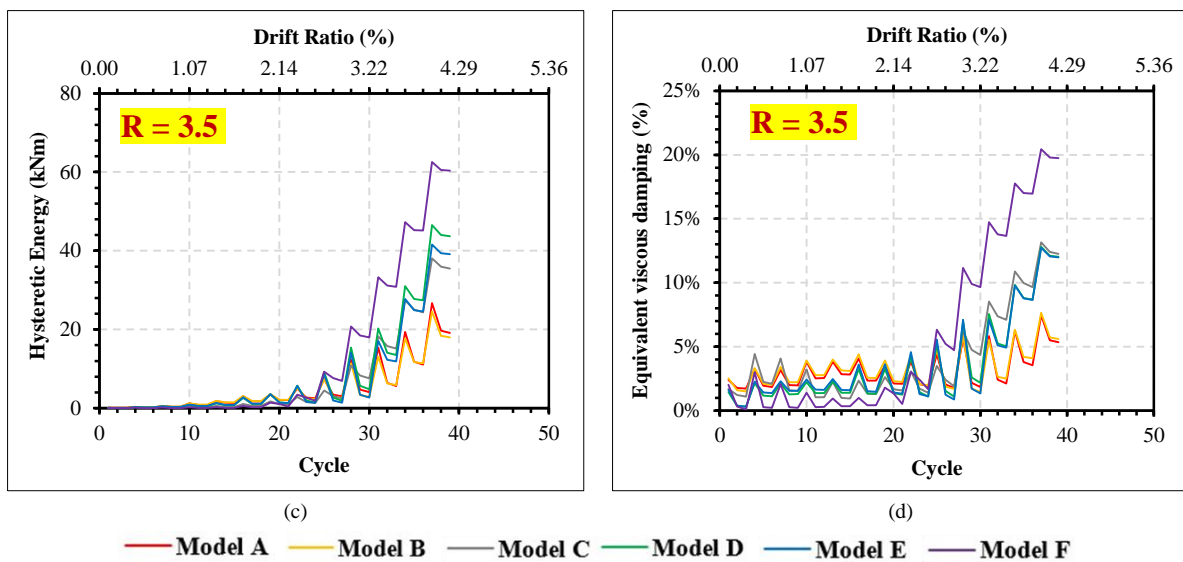

(a)   (b)
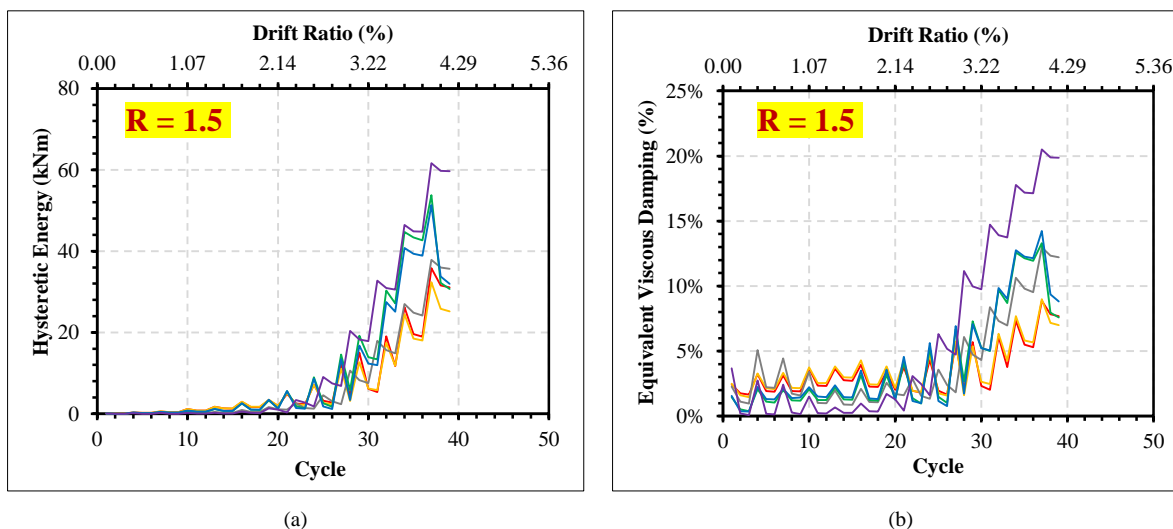
Figure 10. Equal viscous damping and hysteretic energy; (a) Equal viscous damping – R = 1.5, (b) Hysteretic energy – R = 1.5, (c) Equal viscous damping – R = 3.5, and (d) Hysteretic energy – R = 3.5

In another case, it was also discovered that the bored pile models produced the highest equal viscous damping and energy dissipation after exceeding 2% drift. This means ordinary reinforced concrete without prestress had the capacity to achieve a plumper hysteresis loop than the model with prestress due to the absence of initial rebar stress to recover the unloading state. Meanwhile, the bored pile had the lowest equal damping and hysteretic energy below the drift of 2%. It is also important to note that the longer elastic displacement limit and smaller elastic stiffness generated a narrow hysteresis loop under small displacement.

The findings also showed that SPSI models produced higher energy dissipation and equal viscous damping than the bottom-fixed restraint models below 2% drift. It was further discovered that equal viscous damping was generally stable below 5% and under the 2% drift for all models, as shown in Figure 10. Moreover, the results showed that the energy dissipation and equal viscous damping of bottom-fixed restraint models were more significant than the SPSI models after the 2% drift was exceeded. This was due to the fact that the soil spring generated energy dissipation due to plastic deformation under lateral compression of the side surface when the pile experienced low deformation below 2%. However, the increase in deformation led to the absence of significant commensuration in the equal damping of SPSI models with the energy dissipation generated by the bottom-fixed restraint models. The equal viscous damping ratio under large displacement was found to be 3% to 7% and 3% to 12% for the models with and without SPSI, respectively. This aligned with the findings of Cruz & Miranda (2017) [28] that there was a reduction in the damping of the model with SPSI due to the increase in structural height generating insufficient lateral bearing of soil to produce hysteretic damping. Meanwhile, bored pile column models under large displacement achieved equal viscous damping for 3% to 13% and 3% to 20% with and without SPSI, respectively.

The influence of response modification factor (*R*) variation was later clearly shown. The findings showed that the piles with a response modification factor of 1.5 produced higher equal viscous damping and energy dissipation capacities compared to those with a factor of 3.5. Ren et al. (2022) [29] noted that a lighter compression stress level usually leads to a higher PC bar's tensile stress level, and this can lead to higher energy dissipation. The study applied finite element analysis and showed the ability of an increment in the axial force ratio to increase the lateral strength and drift of the hollow spun pile. An increase in the prestressing level of PC bars was also observed in the study to have caused a slight increase in the lateral strength while the lateral drift was reduced. Meanwhile, the spun pile columns designed with an *R*-value of 1.5 in this present study had a lower axial force ratio than *R* of 3.5, which led to a higher equal damping ratio and energy dissipation capacity.

3.2.4. Seismic Performance

The models were observed to have equal levels of seismic performance as indicated by the mean structural response, which was below minimal damage except for Model D with an *R*-value of 3.5. Moreover, the reinforced concrete infill treatment on the top pile generated different trends for the seismic performance of the models with and without SPSI, as shown in Figures 11 and 12. Model A with the SPSI treatment was found to have slightly better seismic performance than Model B without the treatment. Meanwhile, the bottom fixed restraint application using reinforced concrete infill treatment in Model D was discovered to have slightly worse seismic performance than Model E without the treatment. These variations caused different displacement limit states due to the influence of varying plastic hinge proportions and distribution at the top and bottom of the pile, as discussed in previous sections.
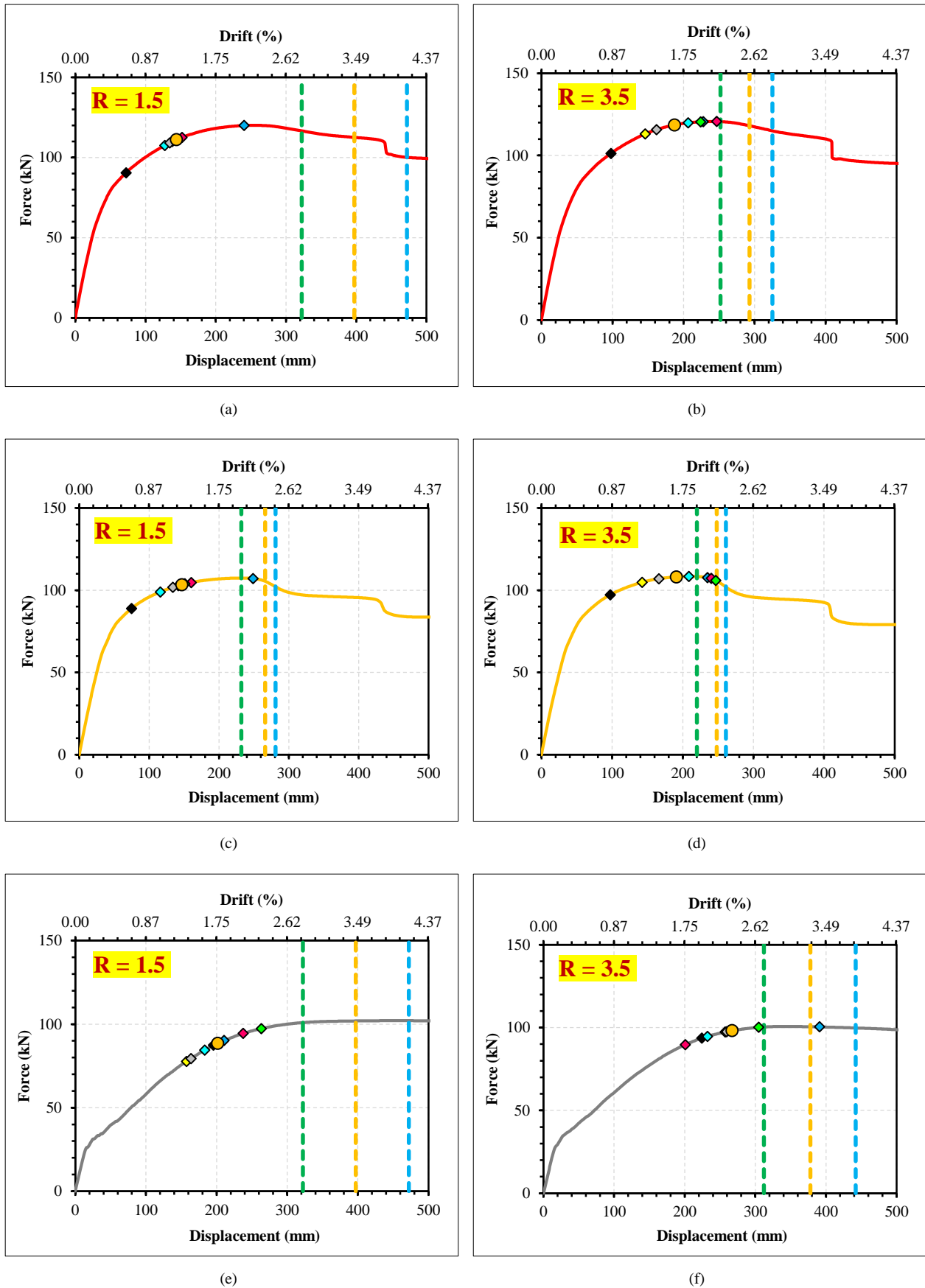
Figure 11. The performance levels of SPSI models; (a) Model A − R = 1.5, (b) Model A − R = 3.5, (c) Model B − R = 1.5, (d) Model B − R = 3.5, (e) Model C − R = 1.5, (f) Model C − R = 3.5
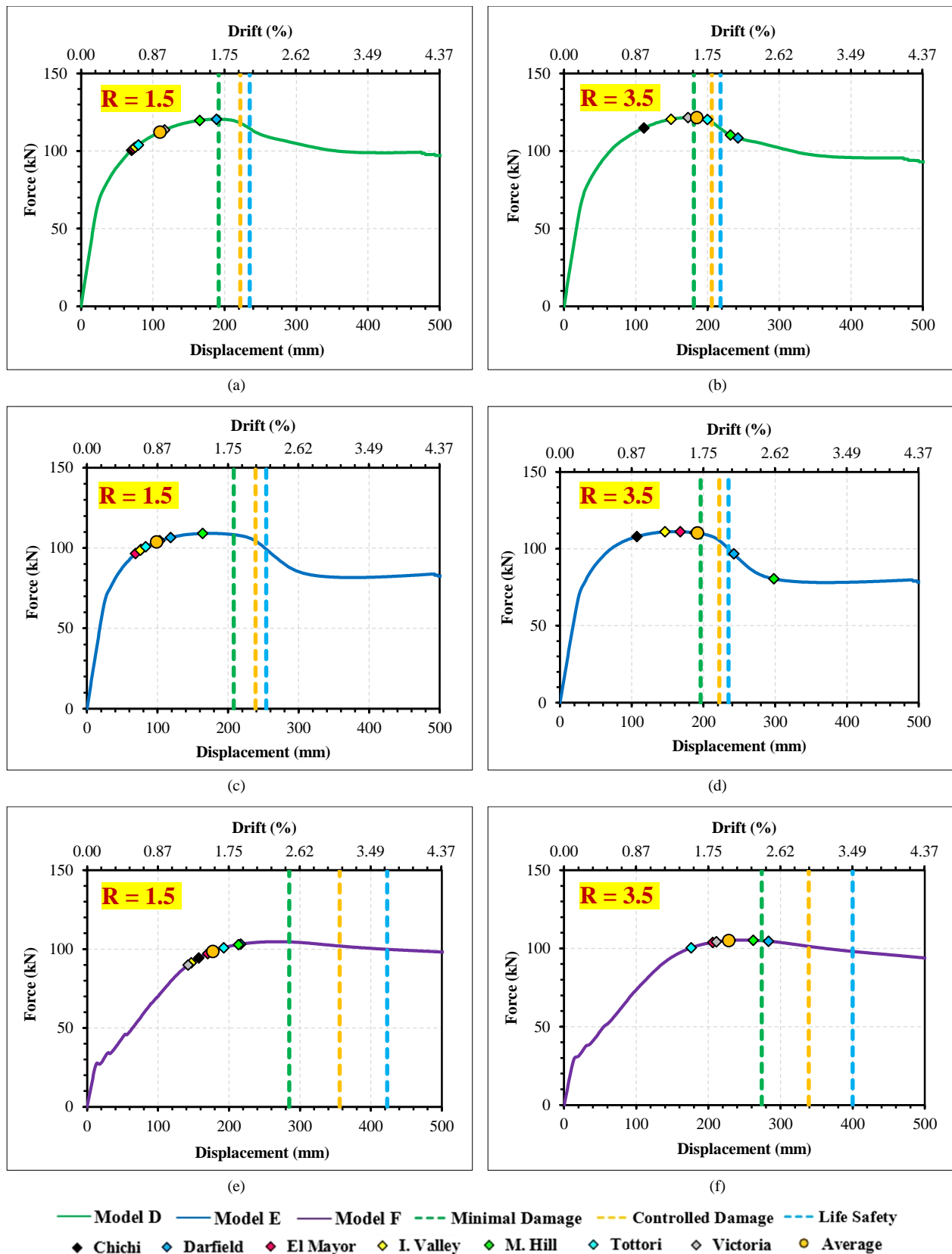
Figure 12. The performance levels of bottom-fixed restrained models; (a) Model D – R = 1.5, (b) Model D – R = 3.5, (c) Model E – R = 1.5, (d) Model E – R = 3.5, (e) Model F – R = 1.5, (f) Model F – R = 3.5

The maximum top-pile displacements of the SPSI models were generally slightly larger than the fixed-base models under seven earthquake excitations based on the backbone curve, the deformation limit state, and the maximum structural displacement response presented in Figures 11 and 12. Meanwhile, the mean maximum top-pile displacements for all the models were below the minimal damage limit except Model D, with a response modification factor of 3.5, which was observed to have a mean response slightly above the minimal damage limit. The implementation of SPSI in

a more flexible structure generated a more significant maximum displacement response due to the general trend of structural spectrum displacement increasing with structural flexibility. Moreover, the SPSI models had better performance in terms of the ratio of displacement response to displacement limit, even though their displacement seismic response was larger than the bottom fixed restraint models.

The implementation response modification factor (R) of 3.5 generated more significant displacement responses than with 1.5, as shown in Figures 11 and 12. However, the 1.5 value was able to maintain the seismic performance below the minimal damage limit, and the maximum displacement response did not exceed the maximum lateral strength of the pile column in all cases with this value. This means the difference in the response modification factors influenced the axial force and mass, and this needed to be supported by every single extended pile column. It is important to note that the implementation of the 3.5 factor in the bottom fixed restraint model generated a higher mean displacement seismic response to the minimal damage limit state. The findings further showed that the performance of some piles exceeded the minimal damage and life safety limits when 3.5 was applied, specifically the spun pile with a fixed bottom restraint. Meanwhile, severe displacement responses that were greater than the life safety limit in Models D and E were caused by the Morgan Hill and Tottori earthquakes.

In comparison, the structural model of the bored pile column with R-values of 1.5 and 3.5 exhibited minimal damage performance, but Model C with 3.5 surpassed the controlled damage performance limit under the Darfield Earthquake. It was also discovered that the bored pile column with an RC concrete section provided adequate energy dissipation and displacement limit, which means it is suitable for use in the SOP viaduct with an R-value of up to 3.5.

In this numerical simulation of a single spun pile column in the SOP viaduct, the macro model idealization only accounted for uniaxial stress-strain behavior (axial-bending stress interaction only) but was not combined with shear stress interactions of the plastic hinge. The effect of varying axial forces due to different pile locations in the global model of the SOP viaduct under earthquake load was also not considered. According to ASCE 61-14, the model of a single spun pile column remains below the minimal damage limit, but there is a possibility of potential premature brittle failure when the maximum lateral strength is exceeded [20]. Irawan et al. (2018) [20] observed this behavior in an experimental study where the spun pile failed due to concrete cover spalling and prestressed bar buckling after reaching its maximum lateral strength capacity. Akiyama et al. (2012) [30] also noted that large lateral forces on the spun pile with reinforced concrete infill had the ability to cause concrete spalling and buckling of longitudinal bars due to their low ductility and flexural capacity. As the standard provisions did not explicitly address the high potential for brittle failure in spun piles, it is advisable to adopt a conservative design approach in practical structural design for SOP viaducts with spun pile columns. It is also recommended to use an R-value of 1.5 in order to ensure a safe structure when resisting the designed earthquake load.

4. Conclusions

The nonlinear analysis conducted to investigate the behavior and seismic performance of single-spun pile columns for the SOP viaduct showed some essential points related to structural engineering knowledge and provided suggestions for practical design, as indicated in the following points.

- In the single-spun pile column model, the top pile treatment with RC infill slightly enforces a larger plastic curvature embedded zone. This led to a slight increase in stiffness, lateral strength, and energy dissipation. The inclusion of SPSI was able to significantly enhance the displacement limit, and this produced better seismic performance compared to the model without this treatment.

- The consideration of SPSI provoked a dominant plastic hinge formation at the top pile, generated a spread distribution at the embedded zone of the pile, and formed medium curvature severity on the top pile compared to the model without considering SPSI. This led to the generation of better energy dissipation under small displacement, less achievement under large displacement, and increased structural flexibility and deformation limits compared to the model without the treatment. It is important to note that the model triggered more significant structural responses under seismic excitations, but the larger displacement limit contributed to better structural performance than without considering the SPSI.

- The application of the 1.5 response modification factor (R) generated a safer spun pile column structure than the 3.5 value in the design to resist earthquake load. This was indicated by the mean structural responses recorded with minimal damage performance in all structural models. Moreover, the consideration of SPSI with an R-value of 3.5 produced seismic performance below minimal damage levels, but some ground motion types triggered structural responses adjacent to the controlled damage performance limit. The findings also showed that the implementation of a bottom fixed restrain with an R-value of 3.5 produced worse seismic performance by exceeding the minor damage level and allowing some structural responses to be greater than the life safety displacement limit.

- It was recommended that a 1.5 R-value should be used for the conservative structural design of the SOP viaduct with spun pile column as long as there is no new standard provided to specifically discuss the best value. There is also the need to consider SPSI in the design to achieve more representative structural behavior to the actual structure.

- There is a need for another study related to the nonlinear analysis of the global model SOP viaduct with consideration for the SPSI in order to enrich more realistic structural behavior and performance. Moreover, the brittle failure mode of the spun pile containing the axial, bending moment, and shear interaction needs to be developed to simulate more detailed structural behavior and performance.

5. Declarations

5.1. Author Contributions

Conceptualization, A.F.S., A.K.S., M.F.D., A.D.A., and S.I.; methodology, A.F.S., A.K.S., M.F.D., A.D.A., and S.I.; validation, A.F.S.; formal analysis, A.F.S., A.K.S., and M.F.D.; writing—original draft preparation, A.F.S., A.K.S., and M.F.D.; writing—review and editing, A.F.S., A.K.S., M.F.D., A.D.A., and S.I.; supervision, A.F.S. All authors have read and agreed to the published version of the manuscript.

5.2. Data Availability Statement

The data presented in this study are available in the article.

5.3. Funding and Acknowledgments

5.4. Conflicts of Interest

The authors declare no conflict of interest.

6. References

[1] Fajar, A. S., Darmawan, M. F., Yogatama, B. A., Satyarno, I., & Guntara, M. (2021). Seismic performance investigation of bracing and SPD application in PHC pile as viaduct piers. The 17th World Conference on Earthquake Engineering, 13-18 September, 2020, Sendai, Japan.

[2] SNI 2833:2016. (2016). Bridge Planning Against Earthquake Loads. Badan Standardisasi Nasional, Jakarta, Indonesia. (In Indonesian).

[3] AASHTO. (2012). AASHTO LRFD Bridge Design Specifications. American Association of State Highway and Transportation Official (AASHTO), Washington, United States.

[4] ASCE 61-14. (2014). Seismic Design of Piers and Wharves. American Society of Civil Engineer (ASCE), Reston, United States.

[5] Putri I. D. & Purwanto T. S. (2018). Planning of slab on pile bridge on Balikpapan Samarinda toll road project (KM. 13 Balikpapan – KM. 38 Sombaja) Segment 1. Ph.D. Thesis, Diponegoro University, Semarang. (In Indonesian).

[6] Mahmoudi, M., & Zaree, M. (2010). Evaluating response modification factors of concentrically braced steel frames. Journal of Constructional Steel Research, 66(10), 1196–1204. doi:10.1016/j.jcsr.2010.04.004.

[7] Berliani, M., Mujiman, & Djuwadi. (2021). Evaluation Experimental of the Dynamic Wharf Structure: A Study Case at Nabire Port, Indonesia. Proceedings of the 2nd International Seminar of Science and Applied Technology (ISSAT 2021), 207. doi:10.2991/aer.k.211106.044.

[8] Budek, A. M., Benzoni, G., & Priestley, M. N. (1997). Experimental investigation of ductility of in-ground hinges in solid and hollow prestressed piles. Report No. SSRP-97/17, University of California, San Diego, United States.

[9] Setiawan, A. F., Darmawan, M. F., Ismanti, S., Mukhlis, S., & Guntara Muria, A. (2020). Numerical model for investigating seismic performance of Prestressed Hollow Concrete (PHC) piles with Fiber section element. E3S Web of Conferences, 156, 03007. doi:10.1051/e3sconf/202015603007.

[10] Cofer, W. F., ElGawady, M., & Greenwood, S. (2009). Seismic Assessment of WSDOT Bridges with Prestressed Hollow Core Piles Part I, No. WA-RD 732.1, Department of Transportation, Washington, United States.

[11] Hutchinson, T. C., Chai, Y. H., Boulanger, R. W., & Idriss, I. M. (2004). Inelastic seismic response of extended pile-shaft-supported bridge structures. Earthquake Spectra, 20(4), 1057–1080. doi:10.1193/1.1811614.

[12] Chai, Y. H., & Hutchinson, T. C. (2002). Flexural Strength and Ductility of Extended Pile-Shafts. II: Experimental Study. Journal of Structural Engineering, 128(5), 595–602. doi:10.1061/(asce)0733-9445(2002)128:5(595).

[13] Mazzoni, S., McKenna, F., Scott, M. H., & Fenves, G. L. (2006). OpenSees command language manual. Pacific earthquake engineering research (PEER) center, University of California, Berkeley, United States.

[14] ASDEA. (2021). Scientific Toolkit for OpenSees (STKO), User Manual, ASDEA SOFTWARE, Pescara, Italy.

[15] Scott, B. D., Park, R., & Priestley, M. J. N. (1982). Stress-Strain Behavior of Concrete Confined By Overlapping Hoops At Low and High Strain Rates. Journal of the American Concrete Institute, 79(1), 13-27. doi:10.14359/10875.

[16] API RP 2A-WSD. (2007). Recommended Practice for Planning, Designing and Constructing Fixed Offshore Platforms-Working Stress Design. American Petroleum Institute (API), Washington, United States.

[17] Boulanger, R. W., Kutter, B. L., Brandenberg, S. J., Singh, P., Chang, D., & University of California, Davis. Center for Geotechnical Modeling. (2003). Pile foundations in liquefied and laterally spreading ground during earthquakes: centrifuge experiments & analyses. No. UCD/CGM-03/01, Center for Geotechnical Modeling, Department of Civil and Environmental Engineering, University of California, Davis, United States.

[18] Darmawan, M. F., Fajar, A. S., Satyarno, I., Awaludin, A., & Yogatama, B. A. (2022). Seismic Performance Comparison of Pile Supported Slab Viaduct with PHC Pile and RC Bored Pile in South Part of Java Island. Proceedings of the 5th International Conference on Sustainable Civil Engineering Structures and Construction Materials. SCESCM 2020, Lecture Notes in Civil Engineering 215. Springer, Singapore. doi:10.1007/978-981-16-7924-7_47.

[19] Kurniawan Santoso, A., Sulistyo, D., Awaludin, A., Fajar Setiawan, A., Satyarno, I., Purnomo, S., & Harry, I. (2022). Structural Systems Comparison of Simply Supported PSC Box Girder Bridge Equipped with Elastomeric Rubber Bearing and Lead Rubber Bearing. Civil Engineering Dimension, 24(1), 19–30. doi:10.9744/ced.24.1.19-30.

[20] Irawan, C., Djamaluddin, R., Raka, I. G. P., Faimun, Suprobo, P., & Gambiro. (2018). Confinement behavior of spun pile using low amount of spiral reinforcement - An experimental study. International Journal on Advanced Science, Engineering and Information Technology, 8(2), 501–507. doi:10.18517/ijaseit.8.2.4343.

[21] Wijesundara, K. K., Nascimbene, R., & Sullivan, T. J. (2011). Equivalent viscous damping for steel concentrically braced frame structures. Bulletin of Earthquake Engineering, 9(5), 1535–1558. doi:10.1007/s10518-011-9272-4.

[22] ASCE 7-10. (2010). Minimum Design Loads for Buildings and Other Structures. American Society of Civil Engineers (ASCE), Reston, United States.

[23] Sunardi, B. (2015). Yogyakarta City Synthetic Soil Acceleration Based on Earthquake Hazard Deaggregation. Journal of Environment and Geological Disasters, 6(3), 211-228. doi:10.34126/jlbg.v6i3.85.

[24] Orientilize, M., Prakoso, W. A., & Swastinitya, A. P. (2021). The different effect of cyclic loading protocol on spun pile performance. IOP Conference Series: Earth and Environmental Science, 622(1), 012011. doi:10.1088/1755-1315/622/1/012011.

[25] El-Arab, I. E., & Maki, T. (2012). Static and dynamic response analysis of reinforced concrete piles. Journal of Civil Engineering and Construction Technology, 3(6), 189-194. doi:10.5897/jcect11.087.

[26] Yang, Z., Li, G., Wang, W., & Lv, Y. (2018). Study on the Flexural Performance of Prestressed High Strength Concrete Pile. KSCE Journal of Civil Engineering, 22(10), 4073–4082. doi:10.1007/s12205-018-1811-y.

[27] Callista, V., Lase, Y., Prakoso, W. A., & Orientilize, M. (2022). Numerical Study of Spun Pile Connections to Pile Caps with and without Fill Concrete Due to Cyclic Loading. Journal Terrace, 12(1), 117. doi:10.29103/tj.v12i1.681.

[28] Cruz, C., & Miranda, E. (2017). Evaluation of soil-structure interaction effects on the damping ratios of buildings subjected to earthquakes. Soil Dynamics and Earthquake Engineering, 100, 183–195. doi:10.1016/j.soildyn.2017.05.034.

[29] Ren, J., Xu, Q., Chen, G., Yu, X., Gong, S., & Lu, Y. (2022). Full - scale experimental study of the seismic performance of pretensioned spun high-strength concrete piles. Soil Dynamics and Earthquake Engineering, 162, 1–17. doi:10.1016/j.soildyn.2022.107467.

[30] Akiyama, M., Abe, S., Aoki, N., & Suzuki, M. (2012). Flexural test of precast high-strength reinforced concrete pile prestressed with unbonded bars arranged at the center of the cross-section. Engineering Structures, 34, 259–270. doi:10.1016/j.engstruct.2011.09.007.